Available online at www.sciencedirect.com

ScienceDirect

Physics Procedia 90 (2017) 399 – 406

Physics Procedia

Conference on the Application of Accelerators in Research and Industry, CAARI 2016, 30 October – 4 November 2016, Ft. Worth, TX, USA

Antihydrogen Beam Formation by Transporting an Antiproton Beam Through an Electron-Positron Plasma That Produces Magnetobound Positronium

M. Hermosillo[a], E. A. Thornton[a], C. A. Ordonez[a]*

[a]*Department of Physics, University of North Texas, Denton, Texas 76203, USA*

Abstract

The formation of an antihydrogen beam by transporting an antiproton beam through an electron-positron plasma that produces magnetobound positronium is studied using a classical trajectory simulation. Through simulation, it is found that antihydrogen can be synthesized via three body recombination involving magnetobound positronium. It has previously been reported that giant cross-magnetic-field particle drifts can occur as a result of binary collisions between charged matter particles and their antimatter counterparts. An electron-positron pair collision can result in a correlated drift of the two particles, perpendicular to a magnetic field. While the two particles remain in their correlated drift, they are referred to as magnetobound positronium. This study was conducted to determine what would happen if a magnetobound positronium system encountered an antiproton. The simulation shows that a positron can be captured into a bound state with an antiproton. This study also considers the effect that the electron-positron collision pitch angle has on antihydrogen production via magnetobound positronium.

Peer-review under responsibility of the Scientific Committee of the Conference on the Application of Accelerators in Research and Industry

Keywords: antihydrogen;positronium; plasma; beam; magnetobound

* Corresponding author. Tel.: +1-940-565-4860; fax: +1-940-565-2515.
E-mail address: cao@unt.edu

Peer-review under responsibility of the Scientific Committee of the Conference on the Application of Accelerators in Research and Industry
doi:10.1016/j.phpro.2017.09.041

1. Introduction

Previous simulations have predicted that within a low temperature plasma that contains electrons and positrons, binary collisions involving electron-positron pairs can cause them to become temporarily correlated and experience giant cross-magnetic field drifts (Aguirre and Ordonez, 2015). Those particle pairs have been referred to as being in a magnetobound state (Correa et al. 2014). It has been previously proposed that magnetobound states may be a useful intermediate state in the production of antihydrogen (Correa et al. 2014). Although various possibilities were discussed in (Correa et al. 2014) concerning possible scenarios in which antihydrogen synthesis could occur via magnetobound states, a simulation of the phenomenon was not reported. This phenomenon occurs at low temperatures and in strong magnetic fields similar to the ones used inside Penning traps that produce antihydrogen. Several collaborations including ALPHA (Charman et al. 2013, Amole et al. 2013, Andersen et al. 2011), ATRAP (Gabrielse et al. 2011-2012, Richerme et al. 2013), ASACUSA (Kuroda et al. 2014), AEgIS (Krasnick et al. 2013), and GBAR (Perez et al. 2012) have achieved or are working towards producing and studying antihydrogen. For example, techniques are being developed to measure the gravitational properties of antihydrogen that could lead to better tests of the gravitational interaction between matter and antimatter (Charman et al. 2013). Furthermore, cooling methods have also been studied that aim to capture cold antihydrogen in strong magnetic fields for precise spectroscopic measurements (Gabrielse et al. 2011). Various alternatives to primary methods that are being used by the CERN collaborations are also being explored (Lane et al. 2014-2016, Ordonez et al. 2012, Rocha et al. 2013). Antihydrogen synthesis via magnetobound states of positronium involves a process that is similar to antihydrogen synthesis via a charge exchange reaction between an excited (e.g., Rydberg) positronium atom and an antiproton. Unlike Rydberg positronium, magnetobound positronium isn't an energetically bound state, because a magnetobound state can dissociated spontaneously and adiabatically. Also, a magnetobound state forms spontaneously and adiabatically from two otherwise free particles that become spatially correlated temporarily as a result of undergoing a collision in the presence of a magnetic field. It is possible that antihydrogen synthesis via magnetobound positronium has previously been simulated but not identified, provided that a free electron, a free positron, and a free antiproton were made available or became available during the simulation so that the phenomenon could occur.

In the work presented here, three body recombination resulting in bound state antihydrogen is studied by computer simulation when a magnetobound positronium system encounters an antiproton. Sec. II discusses the governing equations for the simulation. Sec. III describes the results of the simulation and shows a sample trajectory for a positron captured by the antiproton. Sec. IV contains concluding remarks.

2. Governing Equations

In the simulation, the positron, electron, and antiproton interact classically. The antiproton is approximated as being fixed in space. Beginning with the electric force, Coulomb's law states that the electric force exerted on the positron (particle 1) by the electron (particle 2) is given by $\boldsymbol{F}_{on\,1\,by\,2} = k_c q_1 q_2 \boldsymbol{r}_{12}/r_{12}^3$, where k_c is the Coulomb force constant, q_1 and q_2 are the charges of the positron and electron, $r_{12} = |\boldsymbol{r}_{12}|$ is the distance between particles, and $\boldsymbol{r}_{12} = \boldsymbol{r}_1 - \boldsymbol{r}_2$ is the separation vector between the particles. The Coulomb force constant is $k_c = 1/(4\pi\epsilon_0)$ in SI units, and ϵ_0 is the permittivity of free space. Similarly, the force acting on the positron by the antiproton (particle 3) is $\boldsymbol{F}_{on\,1\,by\,3} = k_c q_1 q_3 \boldsymbol{r}_{13}/r_{13}^3$. These steps are repeated to find the forces acting on the electron. The electric force acting on the electron by the positron is$\boldsymbol{F}_{on\,2\,by\,1} = k_c q_1 q_2 \boldsymbol{r}_{21}/r_{21}^3$, and the electric force acting on the electron by the antiproton is $\boldsymbol{F}_{on\,2\,by\,3} = k_c q_2 q_3 \boldsymbol{r}_{23}/r_{23}^3$.

A magnetic force, $\boldsymbol{F}_B = k_L q(\boldsymbol{v} \times \boldsymbol{B})$, is experienced by each particle. The Lorentz force constant is $k_L = 1$ in SI units, q is the charge of the particle, $\boldsymbol{v}$ is the velocity of the particle, and $\boldsymbol{B}$ is the magnetic field parallel to the unit vector $\hat{\boldsymbol{k}}$. The magnetic force acting on the positron is $\boldsymbol{F}_{on1byB} = k_L q_1 B(v_{1y}\hat{\boldsymbol{\imath}} - v_{1x}\hat{\boldsymbol{\jmath}})$. The unit vectors in a Cartesian coordinate system are $(\hat{\boldsymbol{\imath}}, \hat{\boldsymbol{\jmath}}, \hat{\boldsymbol{k}})$, and v_{1x}, v_{1y}, v_{1z} are the velocity components of the positron. For the electron, $\boldsymbol{F}_{on2byB} = k_L q_2 B\left(v_{2y}\hat{\boldsymbol{\imath}} - v_{2x}\hat{\boldsymbol{\jmath}}\right)$, where v_{2x}, v_{2y}, v_{2z} are its velocity components. Newton's second law governs the classical motion of the particles. For the positron and electron, $\Sigma\boldsymbol{F} = m\boldsymbol{a}$.

Newton's second law for the positron is $\boldsymbol{F}_{on1by2} + \boldsymbol{F}_{on1by3} + \boldsymbol{F}_{on1byB} = m_1\boldsymbol{a}_1$, where m_1 and $\boldsymbol{a_1}$are the mass and acceleration of the positron. Newton's second law for the electron is $\boldsymbol{F}_{on2by1} + \boldsymbol{F}_{on2by3} + \boldsymbol{F}_{on2byB} = m_2\boldsymbol{a}_2$, where

m_2 and $\boldsymbol{a_2}$are the mass and acceleration of the electron. The positron's acceleration is given by $k_c q_1 q_2 \boldsymbol{r}_{12}/r_{12}^3 + k_c q_1 q_3 \boldsymbol{r}_{13}/r_{13}^3 + k_L q_1 B(v_{1y}\hat{\boldsymbol{i}} - v_{1x}\hat{\boldsymbol{j}}) = m_1 \boldsymbol{a}_1$, and the acceleration of the electron is given by $k_c q_1 q_2 \boldsymbol{r}_{21}/r_{21}^3 + k_c q_2 q_3 \boldsymbol{r}_{23}/r_{23}^3 + k_L q_2 B(v_{2y}\hat{\boldsymbol{i}} - v_{2x}\hat{\boldsymbol{j}}) = m_2 \boldsymbol{a}_2$. The position and velocity of a particle are a particle are as $\boldsymbol{r}_i(t) = x_i(t)\hat{\boldsymbol{i}} + y_i(t)\boldsymbol{j} + z_i(t)\hat{\boldsymbol{k}}$ and $\boldsymbol{r}_i'(t) = x_i'(t)\hat{\boldsymbol{i}} + y_i'(t)\hat{\boldsymbol{j}} + z_i'(t)\hat{\boldsymbol{k}}$.

The equations of motion of the positron are

$$\frac{(k_c q_1 q_2 [x_1(t)-x_2(t)])}{\left([x_1(t)-x_2(t)]^2+[y_1(t)-y_2(t)]^2+[z_1(t)-z_2(t)]^2\right)^{\frac{3}{2}}} + \frac{(k_c q_1 q_3 [x_1(t)-x_3(t)])}{\left([x_1(t)-x_3(t)]^2+[y_1(t)-y_3(t)]^2+[z_1(t)-z_3(t)]^2\right)^{\frac{3}{2}}} + k_L B q_1 y_1'(t) = m_1 x_1''(t), \tag{1}$$

$$\frac{(k_c q_1 q_2 [y_1(t)-y_2(t)])}{\left([x_1(t)-x_2(t)]^2+[y_1(t)-y_2(t)]^2+[z_1(t)-z_2(t)]^2\right)^{\frac{3}{2}}} + \frac{(k_c q_1 q_3 [y_1(t)-y_3(t)])}{\left([x_1(t)-x_3(t)]^2+[y_1(t)-y_3(t)]^2+[z_1(t)-z_3(t)]^2\right)^{\frac{3}{2}}} - k_L B q_1 x_1'(t) = m_1 y_1''(t), \tag{2}$$

$$\frac{(k_c q_1 q_2 [z_1(t)-z_2(t)])}{\left([x_1(t)-x_2(t)]^2+[y_1(t)-y_2(t)]^2+[z_1(t)-z_2(t)]^2\right)^{\frac{3}{2}}} + \frac{(k_c q_1 q_3 [z_1(t)-z_3(t)])}{\left([x_1(t)-x_3(t)]^2+[y_1(t)-y_3(t)]^2+[z_1(t)-z_3(t)]^2\right)^{\frac{3}{2}}} = m_1 z_1''(t). \tag{3}$$

The equations of the electron are

$$\frac{(k_c q_1 q_2 [x_2(t)-x_1(t)])}{\left([x_1(t)-x_2(t)]^2+[y_1(t)-y_2(t)]^2+[z_1(t)-z_2(t)]^2\right)^{\frac{3}{2}}} + \frac{(k_c q_2 q_3 [x_2(t)-x_3(t)])}{\left([x_2(t)-x_3(t)]^2+[y_2(t)-y_3(t)]^2+[z_2(t)-z_3(t)]^2\right)^{\frac{3}{2}}} + k_L B q_2 y_2'(t) = m_2 x_2''(t), \tag{4}$$

$$\frac{(k_c q_1 q_2 [y_2(t)-y_1(t)])}{\left([x_1(t)-x_2(t)]^2+[y_1(t)-y_2(t)]^2+[z_1(t)-z_2(t)]^2\right)^{\frac{3}{2}}} + \frac{(k_c q_2 q_3 [y_2(t)-y_3(t)])}{\left([x_2(t)-x_3(t)]^2+[y_2(t)-y_3(t)]^2+[z_2(t)-z_3(t)]^2\right)^{\frac{3}{2}}} - k_L B q_2 x_2'(t) = m_2 y_2''(t), \tag{5}$$

$$\frac{(k_c q_1 q_2 [z_2(t)-z_1(t)])}{\left([x_1(t)-x_2(t)]^2+[y_1(t)-y_2(t)]^2+[z_1(t)-z_2(t)]^2\right)^{\frac{3}{2}}} + \frac{(k_c q_2 q_3 [z_2(t)-z_3(t)])}{\left([x_2(t)-x_3(t)]^2+[y_2(t)-y_3(t)]^2+[z_2(t)-z_3(t)]^2\right)^{\frac{3}{2}}} = m_2 z_2''(t). \tag{6}$$

Prior to the start of the simulation, the electron and positron are treated as traveling in opposite directions towards each other from an infinite distance, and the antiproton is also an infinite distance from both the electron and positron. The electric potential energy is defined to be zero at infinite distances of separation. Conservation of energy requires that,

$$K_{1\infty} + K_{2\infty} = \frac{1}{2}m_1\left(v_{x10}^2 + v_{y10}^2 + v_{z10}^2\right) + \frac{1}{2}m_2\left(v_{x20}^2 + v_{y20}^2 + v_{z20}^2\right) + \frac{k_c q_1 q_2}{r_{120}} + \frac{k_c q_1 q_3}{r_{130}} + \frac{k_c q_2 q_3}{r_{230}}, \tag{7}$$

where v_{x10}, v_{y10}, and v_{z10} are the initial velocity components of the positron at the beginning of the simulation and v_{x20}, v_{y20}, and v_{z20} are the initial velocity components of the electron. The kinetic energies at infinite distances of separation of the positron and electron are $K_{1\infty}$ and $K_{2\infty}$, respectively, and r_{ij0} is the separation between the particles at the start of the simulation. For this simulation, $v_{x10} = v_{x20} = v_{y10} = v_{y20} = 0$, $K_{1\infty} = K_{2\infty} = K_\infty$, $m_1 = m_2 = m$, *and* $v_{z10} = -v_{z20}$.

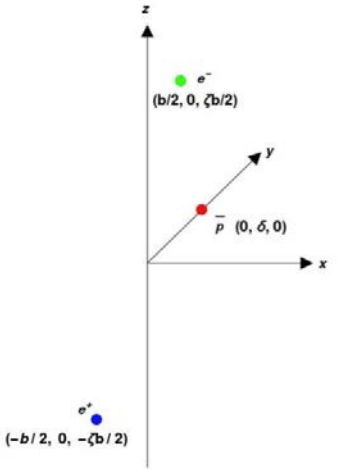

Fig. 1. Initial positions of particles.

Figure 1 shows the initial positions of the particles at the start of the simulation. The electron and positron approach each other with initial velocities that are of equal magnitude but in opposite directions. The simulation begins with the positron at *(-b/2, 0, -ζb/2)*, the electron at *(b/2, 0, ζb/2)*, and the antiproton at *(0, δ, 0)*. This gives $r_{120} = b\sqrt{1+\zeta^2}$, and $r_{130} = r_{230} = \sqrt{(b/2)^2+\delta^2+(\zeta b/2)^2}$. The impact parameter is denoted as b, ζb is the initial axial separation between the electron and the positron, and δ is the distance between the coordinate origin and the antiproton, which is located along the y-axis. Rewriting Eq. (7) provides

$$2K_\infty = mv_{z10}^2 + \frac{k_c q_1 q_2}{b\sqrt{1+\zeta^2}}. \tag{8}$$

Rearrangement of Eq. (8) is used to solve for the nonzero velocity component of the positron at the start of the simulation,

$$v_{z10} = \sqrt{\frac{2K_\infty}{m} - \frac{k_c q_1 q_2}{mb\sqrt{1+\zeta^2}}}. \tag{9}$$

Similarly, the nonzero initial velocity component for the electron is

(10)

$$v_{z20} = -\sqrt{\frac{2K_\infty}{m} - \frac{k_c q_1 q_2}{mb\sqrt{1+\zeta^2}}}.$$

For magnetobound positronium that forms within a plasma environment, the two-body system is equally likely to travel in any direction perpendicular to the magnetic field. The direction of travel is determined by the relative azimuthal orientation of the two particles as they approach one another. In the present work, a coordinate system is oriented such that magnetobound positronium travels toward a nearby antiproton in the y direction, and the coordinate system is in the initial rest frame of the antiproton. The antiproton could be one antiproton of a beam of antiprotons that passes through an electron-positron plasma.

As discussed in (Correa et al. 2014), there are a variety of possibilities for experimentally achieving the phenomenon of antihydrogen synthesis via magnetobound states. The intent of the work presented here is to determine by simulation if, in fact, antihydrogen synthesis via magnetobound states is a new phenomenon. Evaluations of the antihydrogen synthesis rate within specific experimental configurations are beyond the scope of the work presented here, and any commencement of such evaluations should await the conclusion reached in the present study. For the present study, parameters that were previously found to readily produce magnetobound positronium in Ref. 1 are selected. The simulation occurs with the parameters, B = 1 T and $K_\infty = 6\,\kappa$, where κ has the value of Boltzmann's constant in SI units, but with units of energy. The impact parameter b is set equal to $3.1r_c$, due to the large cross-magnetic field drift distance resulting from an electron-positron collision (Aguirre et al. 2015). Here, r_c is the cyclotron radius and is defined as $\sqrt{2K_\infty m/(k_L^2 B^2 q^2)}$. The cyclotron radius is 7.67×10^{-8} m. The trajectories of the positron and electron in a magnetic field were found by solving their equations of motion using a classical trajectory simulation on Mathematica. For a typical simulation, the total energy of the system changed by 7.5×10^{-7} %, and energy was well conserved throughout the simulation.

3. Results

In the simulation, δ was varied from $-100r_c$ to $100r_c$ in increments of 1 r_c. The behavior of the system is chaotic, and there appears to be no specific range of values that will guarantee the positron to be captured by the antiproton. However, preliminary results appear to indicate that capture more reliably occurs when the antiproton is located in the range of $-62r_c < \delta < 32r_c$. Figure 2 shows the electron expelled, while the positron is captured by the antiproton, as projected onto the *yz* plane for $\delta = -45r_c$. Figure 3 shows the positron being captured by the antiproton as projected onto the *xy* plane. Both graphs are normalized by r_c. The process results in the formation of a guiding-center drift atom (Kuzmin et al. 2004).

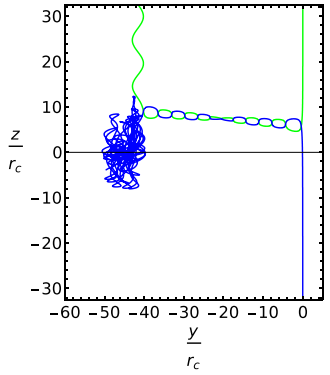

Fig. 2. Projection of the trajectories of the positron (blue) and electron (green) along the *yz* plane.

In addition to a visual inspection of the plotted trajectory of the positron about the antiproton, the total energy of the positron can be examined. For a positron in a bound state, it will have a negative total energy. The positron's total energy includes the kinetic energy due to its motion, the electric potential energy between the positron and the antiproton, and the electric potential energy between the positron and the electron.

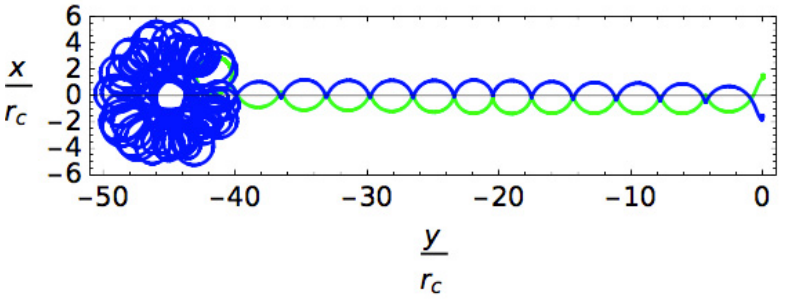

Fig. 3. Projection of the trajectories of the positron (blue) and electron (green) along the *xy* plane.

The value of the electric potential energy between the positron and the electron approaches zero as time approaches infinity, provided the distance of separation between the two particles approaches infinity. As the positron enters a bound orbit, the kinetic energy term and the electric potential energy term stabilize, resulting in a value for the total energy of the positron that approaches a constant negative value as seen in Fig. 4. As a result of the positron's negative total energy and the conservation of energy, the electron therefore carries away excess energy as it is expelled from the system, allowing the formation of antihydrogen to occur.

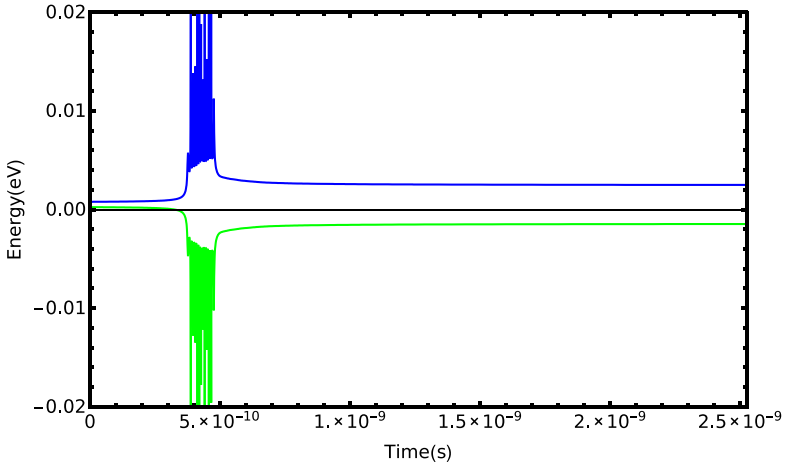

Fig. 4. Graph showing the total energy of the positron (bottom line) and the electron (top line) as a function of time.

A simulation was also developed in which the antiproton was no longer approximated as being fixed in space, and its trajectory was followed. In addition, a nonzero pitch angle between the initial velocity vector and the magnetic field was considered for each lepton. In the simulation, the initial velocity pitch angle θ for the electron was varied from 0° to 90°, while the pitch angle for the positron was set to φ= 45°. The behavior of the system is chaotic and

preliminary results indicate that antihydrogen synthesis occurs more reliably with $\theta \approx 40°$. Figure 5 shows the *yz* axis projection of a successful capture of the positron by the antiproton, while the electron is expelled from the system.

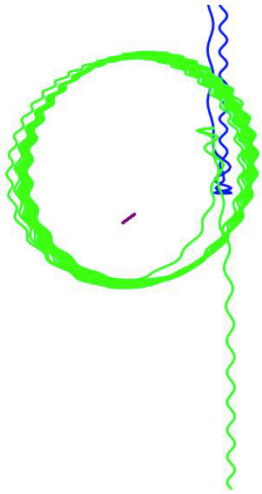

Fig. 5. Same as Fig, 2, except the antiproton trajectory is now simulated starting from rest, and the electron and positron have initial pitch angles of $\theta = 40°$ and $\varphi = 45$, respectively.

4. Conclusion

In conclusion, the simulation demonstrated, both visually and through analysis of the total energy of the positron, the possibility of producing antihydrogen by utilizing magnetobound positronium as an intermediate step. The simulation shows that, as magnetobound positronium drifts across the magnetic field, three-body recombination is possible with an antiproton located along its path to form an antihydrogen atom. The simulation also shows that various initial velocity pitch angles will also allow for recombination to occur.

Acknowledgements

This material is based upon work supported by the National Science Foundation under Grant No. PHYS-1500427 and by the Department of Energy under Grant No. DE-FG0206ER54883.

References

F. F. Aguirre and C. A. Ordonez, Phys. Rev. E 91, 033103 (2015).

C. Amole, M. D. Ashkezari, M. Baquero-Ruiz, W. Bertsche, E. Butler, A. Capra, C. L. Cesar, M. Charlton, A. Deller, S. Eriksson, J. Fajans, T. Friesen, M. C. Fujiwara, D. R. Gill, A. Gutier- rez, J. S. Hangst, W. N. Hardy, M. E. Hayden, C. A. Isaac, S. Jonsell, L. Kurchaninov, A. Little, N. Madsen, J. T. K. McKenna, S. Menary, S. C. Napoli, K. Olchanski, A. Olin, P. Pusa, C. Rasmussen, F. Robicheaux, E. Sarid, C. R. Shields, D. M. Silveira, C. So, S. Stracka, R. I. Thompson, D. P. van der Werf, J. S. Wurtele, A. Zhmoginov, ALPHA collaboration), and L. Friedland, Physics of Plasmas 20, 043510 (2013), http://dx.doi.org/10.1063/1.4801067.

G. B. Andresen, M. D. Ashkezari, M. Baquero-Ruiz, W. Bertsche, P. D. Bowe, E. Butler, C. L. Cesar, S. Chapman, M. Charlton, A. Deller, S. Eriksson, J. Fajans, T. Friesen, M. C. Fujiwara, D. R. Gill, A. Gutierrez, J. S. Hangst, W. N. Hardy, M. E. Hayden, A. J. Humphries, R. Hydomako, S. Jonsell, N. Madsen, S. Menary, P. Nolan, A. Olin, A. Povilus, P. Pusa, F. Robicheaux, E. Sarid, D. M. Silveira, C. So, J. W. Storey, R. I. Thompson, D. P. van der Werf, J. S. Wurtele, and Y. Yamazaki (ALPHA Collaboration), Phys. Rev. Lett. 106, 145001 (2011).

G. B. Andresen, M. D. Ashkezari, M. Baquero-Ruiz, W. Bertsche, P. D. Bowe, E. Butler, P. T. Carpenter, C. L. Cesar, S. Chapman, M. Charlton, J. Fajans, T. Friesen, M. C. Fujiwara, D. R. Gill, J. S. Hangst, W. N. Hardy, M. E. Hayden, A. J. Humphries, J. L. Hurt, R. Hydomako, S. Jonsell, N. Madsen, S. Menary, P. Nolan, K. Olchanski, A. Olin, A. Povilus, P. Pusa, F. Ro- bicheaux, E. Sarid, D. M. Silveira, C. So, J. W. Storey, R. I. Thompson, D. P. van der Werf, J. S. Wurtele, and Y. Yamazaki (ALPHA Collaboration), Phys. Rev. Lett. 106, 025002 (2011).

A. E. Charman, ALPHA Collaboration, and Nature Communications 4, 1785 (2013), http://www.dx.doi.org/10.1038/ncomms2787.
J. R. Correa and C. A. Ordonez, Physics of Plasmas 21, 082115 (2014), http://dx.doi.org/10.1063/1.4894107.
G. Gabrielse, W. S. Kolthammer, R. McConnell, P. Richerme, R. Kalra, E. Novitski, D. Gr- zonka, W. Oelert, T. Sefzick, M. Zielinski, D. Fitzakerley, M. C. George, E. A. Hessels, C. H. Storry, M. Weel, A. Mu¨llers, and J. Walz (ATRAP Collaboration), Phys. Rev. Lett. 106, 073002 (2011).
G. Gabrielse, R. Kalra, W. S. Kolthammer, R. McConnell, P. Richerme, D. Grzonka, W. Oelert, T. Sefzick, M. Zielinski, D. W. Fitzakerley, M. C. George, E. A. Hessels, C. H. Storry, M. Weel, A. Mu¨llers, and J. Walz (ATRAP Collaboration), Phys. Rev. Lett. 108, 113002 (2012).
D. Krasnick, S. Aghion, C. Amsler, A. Ariga, T. Ariga, A. S. Belov, G. Bonomi, P. Brunig, R. S. Brusa, J. Bremer, G. Burghart, L. Cabaret, M. Caccia, C. Canali, R. Caravita, F. Castelli, G. Cerchiari, S. Cialdi, D. Comparat, G. Consolati, L. Dassa, S. Di Domizio, L. Di Noto, M. Doser, A. Dudarev, A. Ereditato, R. Ferragut, A. Fontana, P. Genova, M. Gi- ammarchi, A. Gligorova, S. N. Gninenko, S. D. Hogan, S. Haider, E. Jordan, L. V. Jo/rgensen, T. Kaltenbacher, J. Kawada, A. Kellerbauer, M. Kimura, V. Lagomarsino, S. Mariazzi, V. A. Matveev, F. Merkt, F. Moia, G. Nebbia, P. Ndlec, M. K. Oberthaler, N. Pacifico, V. Petrek, C. Pistillo, F. Prelz, M. Prevedelli, C. Regenfus, C. Riccardi, O. Ro/hne, A. Rotondi, H. San- daker, P. Scampoli, J. Storey, M. A. Subieta Vasquez, M. paek, G. Testera, R. Vaccarone, F. Villa, and S. Zavatarelli, AIP Conference Proceedings 1521, 144 (2013).
N. Kuroda, S. Ulmer, D. J. Murtagh, S. Van Gorp, Y. Nagata, M. Diermaier, S. Federmann, M. Leali, C. Malbrunot, V. Mascagna, O. Massiczek, K. Michishio, T. Mizutani, A. Mohri, H. Nagahama, M. Ohtsuka, B. Radics, S. Sakurai, C. Sauerzopf, K. Suzuki, M. Tajima, H. A. Torii, L. Venturelli, B. Wu¨nschek, J. Zmeskal, N. Zurlo, H. Higaki, Y. Kanai, E. Lodi Rizzini, Y. Nagashima, Y. Matsuda, E. Widmann, and Y. Yamazaki, Nature Communications 5, 3089 (2014), http://dx.doi.org/10.1038/ncomms4089.
S. G. Kuzmin, T. M. O'Neil, and M. E. Glinsky, Physics of Plasmas 11, 2382 (2004).
R. A. Lane and C. A. Ordonez, AIP Advances 4, 077117 (2014), http://dx.doi.org/10.1063/1.4890305.
R. A. Lane and C. A. Ordonez, Journal of Physics B: Atomic, Molecular and Optical Physics 49, 074008 (2016).
C. A. Ordonez and R. M. Hedlof, AIP Advances 2, 012176 (2012), http://dx.doi.org/10.1063/1.3698146.
P. Perez and Y. Sacquin, Classical and Quantum Gravity 29, 184008 (2012).
P. Richerme, G. Gabrielse, S. Ettenauer, R. Kalra, E. Tardi↵, D. W. Fitzakerley, M. C. George, E. A. Hessels, C. H. Storry, M. Weel, A. Mu¨llers, and J. Walz (ATRAP Collaboration), Phys. Rev. A 87, 023422 (2013).
J. R. Rocha, R. M. Hedlof, and C. A. Ordonez, AIP Advances 3, 102129 (2013), http://dx.doi.org/10.1063/1.4827498.